THE SOLAR EUV-EMITTING PLASMA

R. W. NOYES
Smithsonian Astrophysical Observatory and Harvard College Observatory
and
G. L. WITHBROE
Harvard College Observatory, Cambridge, Mass., U.S.A.

1. Introduction

The extreme ultraviolet (EUV) solar spectrum is considered in this review to cover a decade in wavelength from about 300 Å to about 3000 Å. The lower end is close to the practical limit of normal-incidence optics, and the upper end is the approximate limit of visibility from Earth's surface. The solar plasma that gives rise to emission within this interval is very complex and covers a huge range of physical conditions. Temperatures range from about 4×10^3 K (the temperature minimum in the low chromosphere, observed in the 1600 Å continuum) to about 4×10^6 K (corresponding to emission of the Fe XVI doublet at 335 and 361 Å). The density of the emitting plasma ranges from 10^{15} cm^{-3} in the upper photosphere to 10^8 cm^{-3} in the quiet corona. Major types of energy transport and deposition within the plasma include not only radiation, but also acoustic waves, magnetohydrodynamic waves, thermal conduction, and convective flow. Magnetic energy often completely controls detailed structure and energy balances within the plasma. Inhomogeneities are not a small perturbation on the overall structure of the plasma, but rather may completely dominate that structure. Extreme departures from local thermodynamic equilibrium (LTE) are the rule rather than the exception. (It is interesting to contrast this complex situation with that seen in the next wavelength decade, from 3000 Å to 3 μ, which includes the visible spectrum. With the exception of a few strong chromospheric lines, this radiation emerges from a comparatively isothermal (5000 K $< T <$ 6000 K), horizontally homogeneous, atmosphere in hydrostatic and radiative equilibrium, in which LTE is the rule rather than the exception.)

This paper does not attempt a comprehensive review of observations or theories of the solar plasma. Interested readers will find this material covered in recent reviews by Athay (1971), Tousey (1971a, b), and Noyes (1971). In Section 2 we shall review the general characteristics of the quiet solar atmosphere, stressing how the observed emission may be used as a tool to infer this structure. In Section 3 we shall apply many of the same techniques to the study of overall properties of active regions.

2. Physical Conditions in the Quiet Solar Atmosphere

2.1. Mean temperature profile of the chromosphere and corona

Figure 1 illustrates schematically the average run of temperature with height in the chromosphere and low corona, as determined by many investigations, using several

Space Science Reviews **13** (1972) 612–637.

different analytical techniques. The techniques used vary considerably, depending upon the region of the atmosphere being studied.

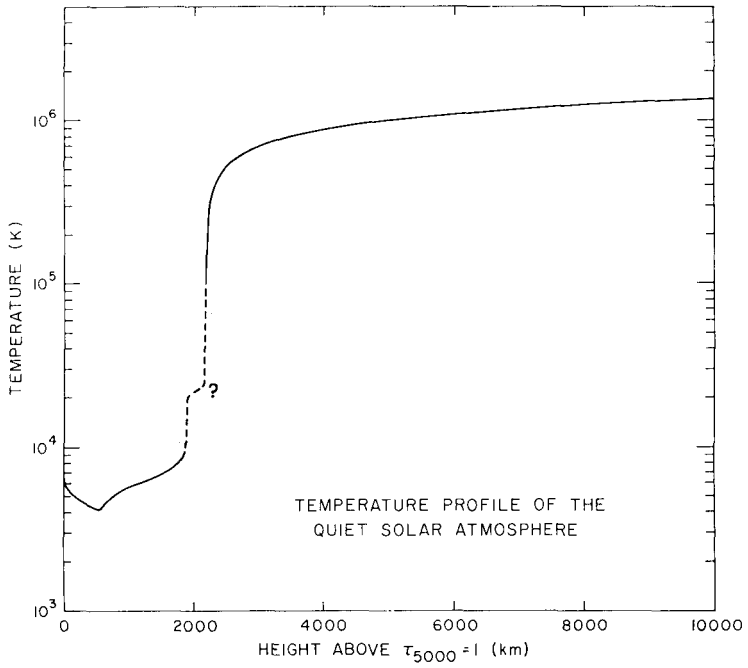

Fig. 1. Schematic diagram of the average run of temperature with height in the chromosphere and low corona.

A. *Temperatures in the Chromosphere from EUV Continua*

Under the assumption of local thermodynamic equilibrium (LTE), the brightness temperature (temperature of a blackbody with equivalent brightness) of the chromosphere is close to the true kinetic temperature of the gas at optical depth unity. Because the observed brightness temperature passes through a minimum near 1600 Å, an absolute measurement of the brightness temperature at that wavelength should yield the minimum kinetic temperature in the low chromosphere.

A minor controversy lives on about the exact value to be assigned to this minimum temperature. Measurements of the ultraviolet continuum near 1600 Å give values ranging from 4300 K to 4600 K (Widing *et al.* 1970; Parkinson and Reeves, 1969). This discrepancy, which corresponds to an intensity difference of a factor of 3, has not been resolved, although independent evidence from the far infrared continuum and from the profiles of the Ca^+ H and K lines suggests the lower value. The 300 K temperature difference, while it may seem trivial, is important in determining the onset of non-radiative heating; a temperature as low as 4300 K is close to the radiative value and would not require that heating be important until above the temperature mini-

https://doi.org/10.1017/S0252921100089788 Published online by Cambridge University Press

mum, whereas the 4600 K temperature would require heating deeper than the temperature minimum (Athay, 1970).

The assumption of LTE at 1600 Å in the silicon continuum has been called into question by Cuny (1971), who calculates that the observed brightness temperature may be nearly 300 K higher than the actual minimum temperature, because the temperature of the ionizing radiation field is higher than the electron temperature at the minimum.

Above the temperature minimum, Cuny's calculations show the opposite effect: the brightness temperature lies below the kinetic temperature at optical depth unity, by an amount that increases with increasing height of formation. Thus the observed 5300 K brightness temperature of the carbon continuum at 1100 Å must be corrected upward by nearly 500 K to give the true kinetic temperature at the 100 km height of formation of this continuum. The non-LTE effects are even more important for the hydrogen Lyman continuum at 912 Å, for which Noyes and Kalkofen (1970) calculated that the observed 6500 K brightness temperature lies nearly 2000 K below the true electron temperature of about 8300 K at optical depth unity. In this case the intensity of the radiation field lies far below the blackbody intensity; the scarcity of ionizing photons causes the hydrogen ground state to be overpopulated by a factor af 200 relative to the LTE value.

In case of the Lyman continuum, one may test such theoretical calculations by observation, for the true electron temperature at optical depth unity may be inferred directly from the energy distribution within the continuum. The Lyman continuum is remarkably free of contamination over a region stretching 100 Å from its head to the violet, and its color temperature (temperature of a blackbody with the same relative energy distribution) has been measured as 8400 K $\pm$ 500 K in the center of the quiet sun (Vernazza and Noyes, 1972). This color temperature is determined by the kinetic energy distribution of the recombining electrons and to a fair approximation is equal to the electron temperature at optical depth unity, for an optically thick continuum. The agreement with the theoretical temperature of 8300 K shows that non-LTE transfer calculations are a useful tool even in the very inhomogenous upper chromosphere.

Directly above unit optical depth in the Lyman continuum, at a height of some 1900 km, the temperature must rise abruptly, to a value at least great enough to provide essentially complete ionization of hydrogen. This is required in order that the overlying layers be transparent, so that the observed radiation can come from a region as cold as that implied by the observed color temperature. At pressures appropriate to the upper chromosphere, the Lyman continuum opacity of neutral hydrogen is so high that essentially all the neutral hydrogen must be removed by ionization within about 100 km above the 8400 K level (Noyes and Kalkofen, 1970).

The steep rise from the level of Lyman continuum emission marks the start of the low transition zone. Above this level significant continuous EUV radiation comes only from the HeI and HeII continua. Their color temperatures can in principle give information on the temperature in the low transition zone, although the problem is not straightforward since they are optically thin (Athay, 1965) and formed in a region

of very steep temperature gradient. In any case, good photometric data are still lacking on the energy distribution within these continua.

However, strong emission from the low transition zone emerges in optically thick lines of neutral, singly-ionized and doubly-ionized light elements such as H, He, C, N, O, Si, and Fe. This emission helps shed light on the important question of whether the temperature rises directly to values in excess of 10^5 K, or whether, as shown in Figure 1, a quasi-isothermal 'plateau' might exist, at temperatures of several times 10^4 K. We have shown the plateau in Figure 1 with a question mark to indicate its presently unsettled status. We now review some of the evidence for and against such a plateau.

B. *Temperature in the Low Transition Zone*, $10^4\ \mathrm{K} < T < 10^5\ \mathrm{K}$

The original suggestion of a plateau in the low transition zone (see Thomas and Athay, 1961, chapter 5) was based on theoretical energy balance considerations: radiation from abundant ions would act as a cooling mechanism and retard the outward temperature rise at those temperatures where the radiative efficiency per unit mass becomes large. Thomas and Athay (1961) concluded that there might exist plateaus associated both with H I emission and with H II emission. Subsequent observations of the flux in the He II lines showed that the latter plateau probably does not exist, but more recent calculations by Athay (1965) reaffirmed that H I Ly α emission could produce a plateau at temperatures in the range 25000 K to 60000 K.

Three separate pieces of observational evidence have recently suggested the possible existence of such a plateau, although at a somewhat lower temperature than suggested by Athay. Each piece of evidence is rather circumstantial, but taken together they merit serious consideration. The evidence is:

(a) Lyman-α and Lyman-β both show large and distinct central reversals (Tousey *et al.*, 1964). Detailed calculations of a model atmosphere with a multi-level hydrogen atom (Vernazza and Avrett, 1972) show that although it is possible to produce the correct intensities of both lines as well as the Lyman-α central reversal without invoking a plateau, the opacity in Lyman-β is insufficient to produce a reversal unless a plateau is introduced, with a width of the order of 100 km if it occurs at 20000 K.

(b) The C II resonance doublet at 1335 Å shows only slight limb brightening. Calculations have shown (Chipman, 1971) that if a model of the low transition zone without a plateau is to reproduce the observed C II intensity, the C II line would have to be formed at about 40000 K and would show roughly twice as much limb brightening as is observed. Only a model such as that in Figure 1 will satisfy both the observed limb brightening and the intensity.

(c) The intensity of the Lyman continuum below 700 Å is at least a factor of two greater than would be contributed by the 8400 K chromosphere. Although the Lyman continuum opacity of a 100 km thick plateau at 20000 K is very small – only 0.02 – the Planck function is so large relative to that at 8400 K that the emission contributed by the plateau just supplies the missing intensity (Vernazza and Noyes, 1972).

The concept of a plateau in the low transition zone with thickness as little as 100 km

is of course rather loose, inasmuch as this is a region with inhomogeneities on a scale much larger than 100 km. Burton *et al.* (1971) have found from analysis of slit spectra above the limb that the emission from neutral and singly ionized elements extends perhaps 7500 km above the mean level of formation of transition zone lines, probably because of the presence of cool spicules at that level. Center-to-limb observations of transition-zone lines at wavelengths shorter than 912 Å (Withbroe, 1970a) show that those spicules that penetrate the transition zone contain enough cool material to be opaque in the Lyman continuum. Thus the plateau described above may well have meaning only in a statistical sense.

Some evidence argues against the existence of such a plateau. Burton *et al.* (1971) have concluded that the thickness of the region between 10^4 K and 10^5 K is only about 75 km, based on emission measures of lines formed in this region, as we describe below. Thus the question of the plateau is very much open, and may well remain so until observations with higher spatial resolution are obtained and analyzed.

C. *Temperature in the Upper Transition Zone, $T > 10^5$ K*

Above 10^5 K, most lines are optically thin and radiative transfer is no longer important. In addition the density is low enough that population of excited levels generally does not affect collisional ionization rates; under these conditions all ionization and recombination rates depend quadratically on the density, and hence the ionization equilibrium ratios between different ions are density independent. Emission measures can be calculated in a straightforward fashion under such conditions.

Several authors (e.g., Pottasch, 1963; 1964; 1967; Jordan, 1965; Athay, 1966; Dupree and Goldberg, 1967; Dupree, 1971) have derived models of the transition zone using slight variants of the emission measure analysis developed originally by Ivanov-Kholodnyi and Nikolskii (1961) and Pottasch (1963). The flux emitted by a collisionally excited EUV line is

$$E = \text{const}\, A \int_0^\infty n_e^2 G(T)\, \mathrm{d}h\,, \tag{1}$$

where A is the abundance of the element producing the line, n_e is the electron density, $G(T)$ is a temperature-dependent function that depends upon the ionization and excitation properties of the atom producing the line, and h is height. Athay (1966) factored the quantity $P = n_e T$ outside of the integral on the grounds that the geometrical thickness of the transition zone is far less than a pressure scale height and the pressure is therefore essentially constant across the transition zone. Assuming that the temperature gradient $\mathrm{d}T/\mathrm{d}h$ is constant over the relatively narrow range of temperature in which an individual ion can exist, one may also factor out the mean inverse temperature gradient and rewrite Equation (1) as

$$E = \text{const}\, A P^2 \langle (\mathrm{d}T/\mathrm{d}h)^{-1} \rangle \int_0^\infty \frac{G(T)}{T^2}\, \mathrm{d}T\,. \tag{2}$$

https://doi.org/10.1017/S0252921100089788 Published online by Cambridge University Press

The integral in Equation (2) may be evaluated for each emission line independently of the atmospheric model. Through use of a variety of lines formed at different temperatures, one can then obtain $\langle(\mathrm{d}T/\mathrm{d}h)^{-1}\rangle$ as a function of $\langle T\rangle$, the mean temperature of line formation, providing the pressure P is known. Integration of the resulting relationship between temperature gradient and temperature yields the run of temperature with height.

As we mentioned earlier, Burton *et al.* (1971) applied this technique to the low transition zone ($10^4\ \mathrm{K} < T < 3\times10^5\ \mathrm{K}$) and derived a model of this region in which the temperature rises from 10^4 K to 10^5 K in only 75 km. Although many of the lines used in their analysis are optically thick, they are 'effectively thin'; that is, collisionally produced photons escape after repeated scatterings, without being destroyed by collisional de-excitation or other transitions out of the upper level. Equation (1) is applicable to such lines.

In the upper transition zone, between approximately 10^5 K and 10^6 K, where the temperature gradient is also very steep, the temperature structure appears to be governed primarily by the conduction of heat from the corona to the chromosphere. This was pointed out by Athay (1966) in an analysis of EUV flux measurements. He found that the temperature gradient in the upper transition zone was proportional to $T^{-5/2}$; this would be expected for an atmosphere in which the temperature gradient adjusts to the variation of the thermal conductivity $\varkappa$ such that the conductive flux remains constant throughout the region. Application of the recent determination of $\varkappa$ by Ulmschneider (1970) to models of the transition region developed from analysis of EUV flux measurements (Dupree and Goldberg, 1967) and intensities at the center of the quiet sun (Withbroe, 1970a; Dupree, 1971; Dupree and Reeves, 1971) gives a conductive flux from the corona to the chromosphere of approximately 10^6 erg cm^{-1}s^{-1}.

Another method of determining the temperature structure in the upper transition zone and corona involves comparing observations of EUV lines at disk center and in the corona above this limb. It can be shown (Withbroe, 1970a) that the ratio of intensities above the limb to those at disk center for lines formed partially in the transition layer and partially in the corona depends upon the coronal temperature and the temperature gradient in the transition zone. The coronal temperature can be determined from the observations above the limb of ratios of lines in different stages of ionization. For quiet areas a coronal temperature of 1.8×10^6 K appears to be consistent with EUV intensities measured several arc minutes above the limb (Withbroe, 1970a; 1971a). If the temperature gradient in the upper transition region ($10^5\ \mathrm{K} \lesssim T \leqslant 10^6\ \mathrm{K}$) is given by $\mathrm{d}T/\mathrm{d}h = C^{-1}\ T^{-5/2}$, as seems reasonable from analyses of EUV flux data (Athay, 1966; Dupree and Goldberg, 1967) and intensity data (Dupree, 1971), then the ratio of intensities above the limb to those at disk center gives $C = 10^{-12}$ (Withbroe, 1970a). This corresponds to a conductive flux of 10^6 erg cm^{-1} s^{-1} in agreement with the analyses of flux and intensity data.

2. 2. Direct measurement of heights in the solar atmosphere

One problem in deriving models for the transition zone from absolute flux or intensity

https://doi.org/10.1017/S0252921100089788 Published online by Cambridge University Press

measurements is that the relationship between heights in the models and height above the solar surface is not defined. Several techniques have been used to establish this relationship. The simplest method has been to fit the temperature curve for the transition zone to the steeply rising portion of the temperature curve in the upper chromosphere. This results in a transition zone located about 2000 km above the solar surface (cf. Athay, 1966; Noyes and Kalkofen, 1970; Gingerich *et al.*, 1971). This method of establishing a height scale rests on the assumption of hydrostatic equilibrium, which is clearly open to some question in view of the large non-thermal velocity fields known to exist in the chromosphere and above. Corrections for turbulent pressure are uncertain because of our imperfect knowledge of the detailed height dependence of the velocity field. Therefore direct measurements of height of EUV emission are highly desirable.

One time-honored method of directly measuring heights in and above the chromosphere uses eclipse measurements, in which the regular motion of the Moon's limb projected on the solar limb provides a precise and absolute height scale. Differentiation of the run with time of total intensity above the limb observed on chromospheric flash spectra can in principle yield heights accurate to within a fraction of an arc sec, or a few hundred km. Data that may permit this type of analysis in the EUV were obtained at the March 7, 1970, solar eclipse (Speer *et al.*, 1970; Gabriel *et al.*, 1971; Brueckner *et al.*, 1970); these data are presently under analysis.

Burton *et al.* (1971) have attempted direct measurements of heights in the transition zone from analysis of slit spectra obtained at disk center and at the solar limb. For optically thin lines, the ratio of flux entering the spectrograph slit at the limb to that at disk center is dependent only on the geometry of the emitting layer in the solar atmosphere projected on the spectrograph entrance slit. Differences in the limb-disk ratio for different lines may be directly related to differences in height of emission of these lines in the solar atmosphere. Burton *et al.* found that, as predicted by models of the transition zone, all lines formed in the transition zone occur at the same height to within the uncertainties of their data, about one arc sec or 700 km. However, because the precise location of the spectrograph slit relative to the limb is uncertain, the absolute height of the transition zone could not be obtained.

Withbroe (1970b) inferred the absolute height of the transition zone from the effects of absorption by chromospheric spicules on transition zone lines observed near the limb. Below 912 Å, spicules appear to be opaque in the Lyman continuum. From the known number-density and dimensions of spicules, it was possible to calculate the absorption near the limb of an emitting layer that lies below the tops of the spicules. The amount of absorption depends on the height of the emitting layer since the number of spicules above a given height decreases with height. Withbroe found from the observed absorption that the steep part of the transition zone lies about 2000 km above the limb, in good agreement with model calculations.

A different technique was recently used by Simon and Noyes (1972), who measured the distance between the brightest points in pairs of active regions separated by large fractions of the solar diameter. This separation, projected on the disk, is proportional

to the distance of the emitting regions from the center of the Sun; thus changes in the distance found when observations are made in different lines directly reflect height differences. The heights of emission of EUV lines in active regions found in this way are in good agreement with model calculations, suggesting that even in active regions, hydrostatic equilibrium is a useful assumption. The method has so far been applied only to low resolution (1′) EUV data, but holds promise for later application to higher resolution data.

2. 3. Density determinations in the solar atmosphere

Densities in the chromosphere, transition zone, and lower corona are generally computed as a function of height through use of the assumption of hydrostatic equilibrium, with the density specified at some height. A useful parameter is the pressure, $P=n_eT$, which in hydrostatic equilibrium models is nearly constant in the upper chromosphere and transition zone. For the mean quiet Sun n_eT appears to be between 5×10^{14} and 1.5×10^{15}, as we shall see below.

Calculation of the EUV spectrum of the chromosphere requires a complete solution of the equation of statistical equilibrium, including all relevant radiative and collisional processes. To the extent that collisional processes are important, it is possible to place restrictions on density in the region of emission. One example is provided by the carbon and hydrogen bound-free continua, in which departures from LTE, and hence the observed brightness temperatures, have been found to depend on electron density (Cuny, 1971; Noyes and Kalkofen, 1970).

Observations of line ratios of optically thick chromospheric lines also provide information on densities, but here the problem is complicated by the necessity of not only calculating the collisional rates between atomic levels, but also including the effect of optical thickness on the level populations. One example of the complexity that may be attained in such an analysis is provided by the work of Hearn (1969), who interpreted measurements of the helium resonance lines at 584 and 537 Å using a 41-level model helium atom. Hearn found that the ratio of intensities at 584 Å and 537 Å is sensitive to electron density as well as to optical depth in the lines. Using OSO-4 data Hearn *et al.* (1969) found the quiet region density at a temperature of 3×10^4 K to be about 4.5×10^{10} cm^{-3}, leading to a pressure $P=n_eT$ of 1.4×10^{14} in the upper chromosphere. This pressure is a factor of 2 higher than that used by Noyes and Kalkofen (1970) in their analysis of the hydrogen Lyman continuum.

The densities on present models of the transition zone and lower corona of the quiet sun (e.g. Pottasch, 1964; 1967; Athay, 1966; Dupree and Goldberg, 1967; Withbroe, 1970a; Burton *et al.*, 1971) are based on chromospheric and coronal electron densities derived from observations in the visible. The latter observations suggest that n_eT in the transition zone is approximately 6×10^{14} to 10^{15} (Pottasch, 1964; Jordan, 1965; Athay, 1966; Withbroe, 1970a, 1971a). This method of determining densities in the transition zone is indirect because it depends upon knowledge of densities above or below the transition zone and upon the assumption of hydrostatic equilibrium.

It is possible to determine more directly the electron density in the transition zone by using EUV line ratios that are density sensitive. As has been discussed elsewhere in this symposium (Kunze, 1972; also see Dupree *et al.*, 1971; Jordan, 1971; Munro *et al.*, 1971), level populations of ions with metastable levels are often rather sensitive to electron density; radiative and collisional transitions into and out of metastable levels may occur at comparable rates, and the equilibrium population depends on which is dominant. A good example is provided by ions of the beryllium iso-electronic sequence. Figure 2 (Munro *et al.*, 1971) shows the population of the metastable triplet

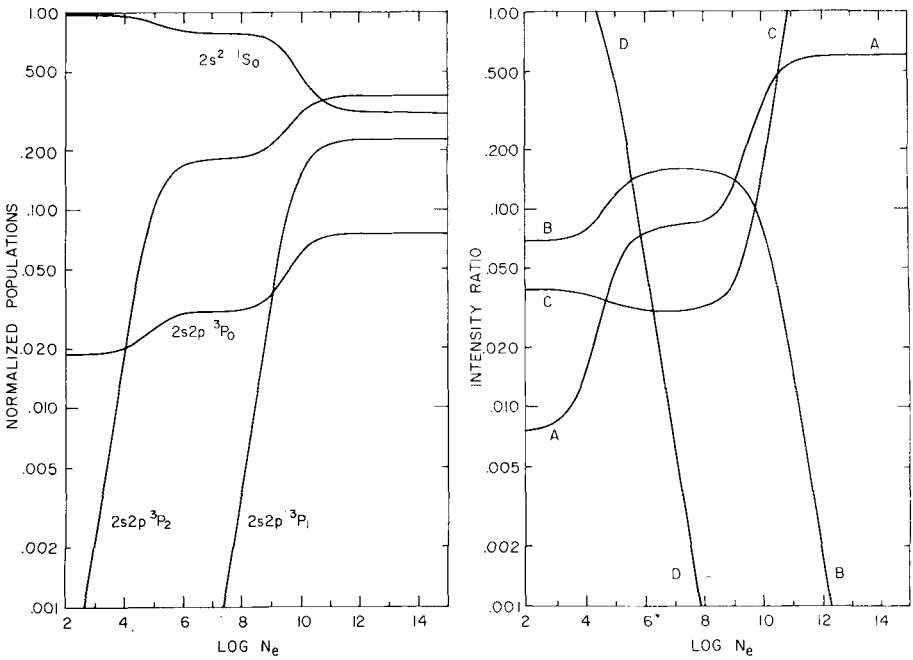

Fig. 2. (left) Normalized populations of the ground and metastable levels of C III as a function of electron density. (right) Corresponding relative intensities (in ergs cm^{-2} s^{-1} sr^{-1}). Curve A: I(1176 Å)/I(977 Å); B: I(1909 Å)/I(977 Å); C: I(1907 Å)/I(1909 Å); D: I(2298 Å)/I(1909 Å)

levels of the beryllium-like C III ion, relative to that of the ground state. Plateaus of nearly constant relative population occur when the electron density reaches values sufficient for collisions to counteract the radiative depopulation of the $^3P_0$, $^3P_2$, and $^3P_1$ hyperfine levels. Figure 2 also shows the resulting variations of various emission line ratios, including the well-observed ratio of the ^3P–^3P and ^1P–^1S lines (at 1176 Å and 977 Å in C III). The regions of steep density-dependence of this ratio include densities appropriate to the transition zone in the quiet Sun. The same ratio in the iso-electronic O V ion is rather density-sensitive at densities appropriate to active regions, but is relatively insensitive to density in the quiet Sun. The pressure n_eT inferred for the quiet transition zone from OSO–6 observations of the C III lines is about 6×10^{14} (Munro *et al.*, 1971), in good agreement with pressures obtained by other means.

https://doi.org/10.1017/S0252921100089788 Published online by Cambridge University Press

Chipman (1971) has analyzed OSO–4 observations of the absolute intensities and limb brightening of C III 977 Å and C III 1176 Å and obtained a self-consistent quiet-Sun model explaining the observations with $n_e T = 4 \times 10^{14}$.

Another technique for determining densities from EUV data uses the observations of lines from different stages of ionization to construct models of the transition zone and lower corona that are defined by several parameters. One such model is the three-parameter model (Withbroe, 1970a; Noyes *et al.*, 1970) discussed earlier, in which the temperature structure is fixed by setting the temperature gradient in the transition region equal to $C^{-1} T^{-5/2}$ and fitting onto the transition zone an isothermal corona with a temperature T_c. The run of density with height is determined by the hydrostatic equilibrium equation and the pressure $P = n_e T$ at $T = 10^5$ K. Through comparison of observed EUV emission from different ions and theoretical intensities calculated with a family of models, it is possible to derive values for C, T_c and P (Withbroe and Noyes, 1971). Reimers (1971) has developed a similar technique for a one-parameter model that depends upon specifying the conductive flux from the corona to the chromosphere. For the quiet Sun the mean value of $n_e T$ derived by fitting these simple models to OSO-6 EUV measurements of N V, O VI, Ne VIII, Mg X, and Si XII lines is approximately 10^{15} (Withbroe and Noyes, 1971). For limb observations with moderate spatial resolution 1′ the densities inferred from EUV data are consistent with those inferred from observations of the brightness of the white light K corona (Withbroe, 1971a).

2.4. Chemical composition of the transition zone and lower corona

There has been considerable discussion about the chemical composition of the solar atmosphere and the possibility that the photosphere and the higher layers of the atmosphere differ in composition. A major problem has been the apparent order-of-magnitude difference between the photospheric and coronal iron abundances. This problem has now been largely resolved by improved oscillator strenghts (see Garz and Koch, 1969; Bridges and Wiese, 1970), which resulted in a large upward revision in the photospheric iron abundance (e.g. Garz *et al.*, 1969).

Solar abundances have been derived from EUV data by a number of authors (e.g. Pottasch, 1963, 1964, 1967; Jordan, 1966; Athay, 1966; Dupree and Goldberg, 1967; Jordan and Pottasch, 1968; Nikolskii, 1969; Reimers, 1971; Dupree, 1971; Withbroe, 1970a, 1971a, 1971b). Since these papers describe the techniques for deriving chemical abundances from EUV data, we will not present a detailed discussion here. Relative abundances can be determined by comparing relative intensities of lines that are formed in the same temperature range but come from different elements. Relative abundances can be placed on an absolute scale, that is, a scale relative to hydrogen, through use of a combination of EUV and radio observations or EUV and K-corona observations. Table I lists abundances for the transition zone and lower corona. These abundances, taken from a recent review of the solar chemical composition (Withbroe, 1971b), were determined from EUV data. The absolute scale is based on comparisons of EUV and radio data (Pottasch, 1963, 1964, 1967; Dupree and Goldberg, 1967; Neupert, 1967; Reimers, 1971) and a comparison of EUV and K-coronameter data (With-

broe, 1970, 1971a). An absolute scale with $\log N_{Si} = 7.5$ where $\log N_H = 12.0$ best represents the results of these studies.

For comparison with the transition zone and coronal abundances, Table I also lists photospheric values (Withbroe, 1971b). The two sets of abundances are in sufficiently good agreement that it seems appropriate to adopt the hypothesis that they are equal, until better evidence to the contrary is found.

TABLE I

Solar chemical composition

Atomic No.	Element	Abundances[a]	
		Transition zone and corona	Photosphere
1	H	12.0	12.0
6	C	8.6	8.57
7	N	7.9	8.06
8	O	8.6	8.83
10	Ne	7.4	
11	Na	6.3	6.24
12	Mg	7.5	7.54
13	Al	6.3	6.40
14	Si	7.5	7.55
15	P	5.3	5.43
16	S	7.2	7.21
18	Ar	6.5	
20	Ca	6.2	6.33
26	Fe	7.5	7.40
28	Ni	6.5	6.28

[a] Log $N_A + 12.0$ where N_A is the abundance of the element relative to hydrogen. Values from Withbroe (1971b).

Delache (1967) has pointed out that thermal diffusion can affect the relative chemical composition in different layers of the solar atmosphere. Since there are uncertainties in the abundances given in Table I, amounting to the order of 0.3 dex, the apparent agreement between the photospheric and transition zone abundances does not rule out the possibility of diffusion effects.

2. 5. Energy Balance and the Problem of Inhomogeneities

Given the run of temperature and density with height, as well as the chemical composition, one can calculate two of the most important energy fluxes in the chromosphere and corona: the radiative flux and the thermal conduction. The radiative losses from a gas of solar composition were calculated as a function of temperature by Cox and Tucker (1969) and recently updated by Boland *et al.* (1972), to take account of the increased iron abundance. The conductive fluxes may be calculated from the relation $F_c = -\varkappa(dT/dh)$, where the thermal conductivity $\varkappa$ may be approximated by $\varkappa = 1.75 \times$

$\times 10^{-6} \cdot T^{5/2} P^{0.04}$, for temperatures in excess of 20000 K (Ulmschneider, 1970). In this equation p is the gas pressure, and all quantities are in cgs units.

It is beyond the scope of this article to discuss in detail the energy balance in the chromosphere and corona; a good discussion of this important problem has been given recently by Athay (1971). We simply note here that the energy balance question lies at the core of our understanding the physics of the chromosphere and corona. Because radiation and conduction are major energy transfer processes, much qualitative progress in understanding the energy balance has resulted from the studies reviewed above. However, a detailed description of the energy balance awaits a number of observations which have not yet been obtained. Among these are:

(a) Detailed studies of the velocity field, from measurements of Doppler shifts of EUV lines and of velocity-broadened line profiles. These measurements are important to determine the mechanical flux in acoustic waves or shocks, and to study the bodily transport of both mass and kinetic energy in moving elements such as spicules or their coronal counterparts. The beginnings of such studies have been made from observations of non-thermal line broadening (see, e.g. Boland *et al.*, 1972), but because of the highly inhomogeneous velocity field expected, high spatial resolution is mandatory.

(b) Detailed measurements of the magnetic field in the photosphere and as high in the atmosphere as possible. Because even a rather weak field completely inhibits thermal conduction perpendicular to the field lines, a knowledge of the fine-scale three-dimensional structure of the field in the upper atmosphere is very important. Although one can extrapolate the photospheric field into the corona, assuming a current-free configuration (Schmidt, 1964; Altschuler and Newkirk, 1969), such an assumption is not generally valid. Unfortunately, observations of the field in the chromosphere or corona are extremely difficult.

(c) Observations of emission measures of EUV lines with high spatial and temporal resolution. We have seen how low-resolution observations of EUV intensities yield information to determine mean values of radiative and conductive fluxes. However, the transition zone and corona are inhomogeneous on a scale at least as fine as a few arc sec. Until we can determine the structure on that scale, detailed calculations of energy balance will remain highly speculative.

Observations with high temporal resolution may be useful in revealing the response of the atmosphere to rapid or periodic energy deposition, such as might be produced by the passage of shock waves. Thus, even if the shock waves could not be seen directly through their velocity fields, they might be revealed through their effects on the atmosphere.

Although EUV data with both high spatial and high temporal resolution are not yet available, some very important EUV observations have been obtained showing the fine structure in the chromosphere and transition zone. Figure 3 shows two images from a 1968 NRL rocket flight (Tousey, 1971a). The chromospheric network prominent at about 7000 K in the Ca II K line is seen to be extremely bright in He I 304 Å at about 60–80000 K; it is also pronounced in O V 630 Å at 250000 K. The network appears weakly in Mg X 625 Å at 1.4×10^6 K as seen in moderate-resolution OSO-6

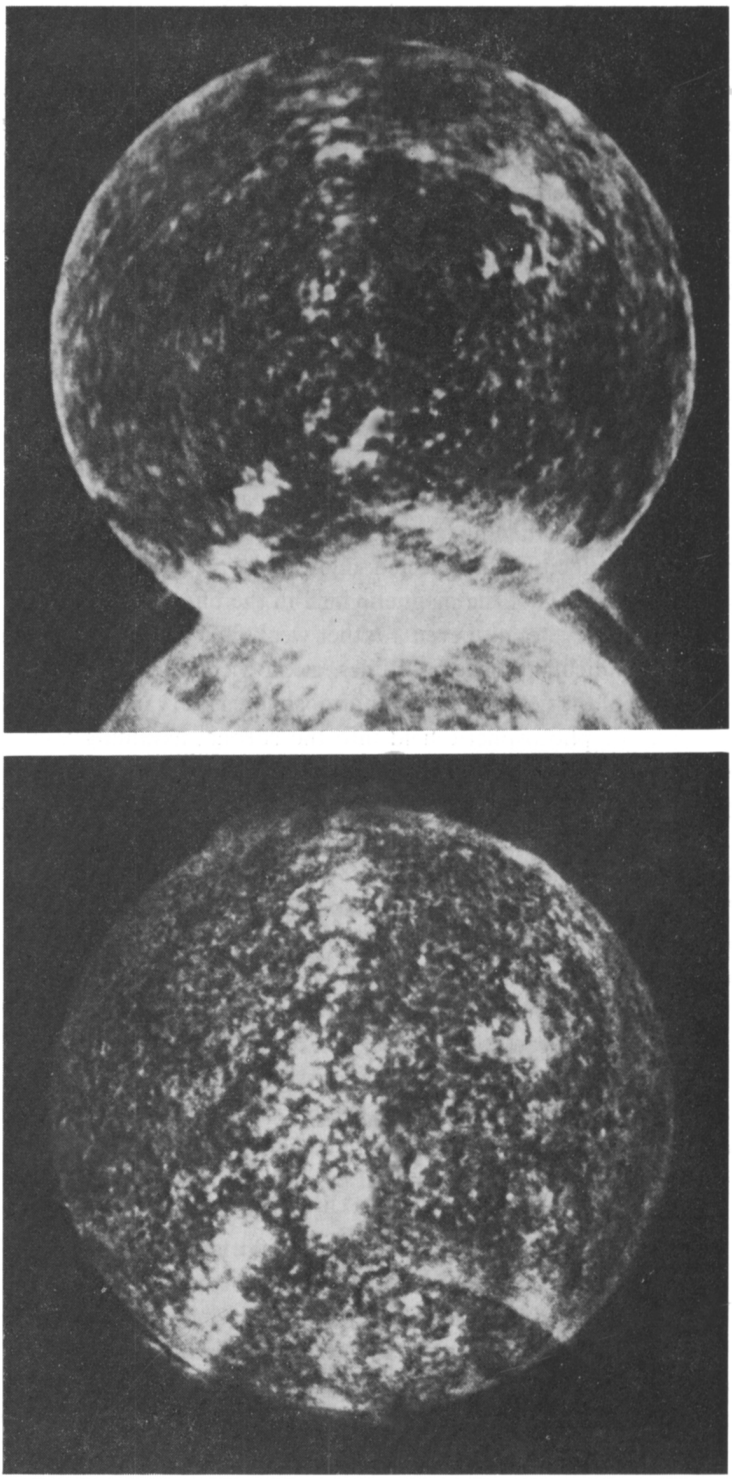

Fig. 3. Naval Research Laboratory spectroheliograms in He II 304 Å (left) and O V 630 Å (right). (Courtesy Naval Research Laboratory.)

https://doi.org/10.1017/S0252921100089788 Published online by Cambridge University Press

observations (Reeves and Parkinson, 1972), but observations of the quality of Figure 3 are not yet available. It will be of the greatest interest to obtain observations throughout the atmosphere to measure the density, temperature, and size of the network with height. Calculations by Kopp and Kuperus (1968) suggest that the magnetic field associated with the network will channel the heat conducted from the corona into the network boundaries and produce widely different temperature-density structures in the interiors and in the boundaries of network cells. The EUV observations to be obtained by future rocket, OSO, and ATM experiments should resolve these structures and lead to more sophisticated and realistic quiet-Sun models than those presently available.

3. Structure of Active Regions From EUV Data

We now turn to an area where observations with only moderate spatial resolution can still be of great importance, the study of active regions. Active regions appear to be associated with a large increase of heat flow into the chromosphere and corona. Even if we are not yet able to describe the detailed mechanism responsible for the heating, we can use observations of active regions as a probe to explore what happens when such a basic parameter is altered.

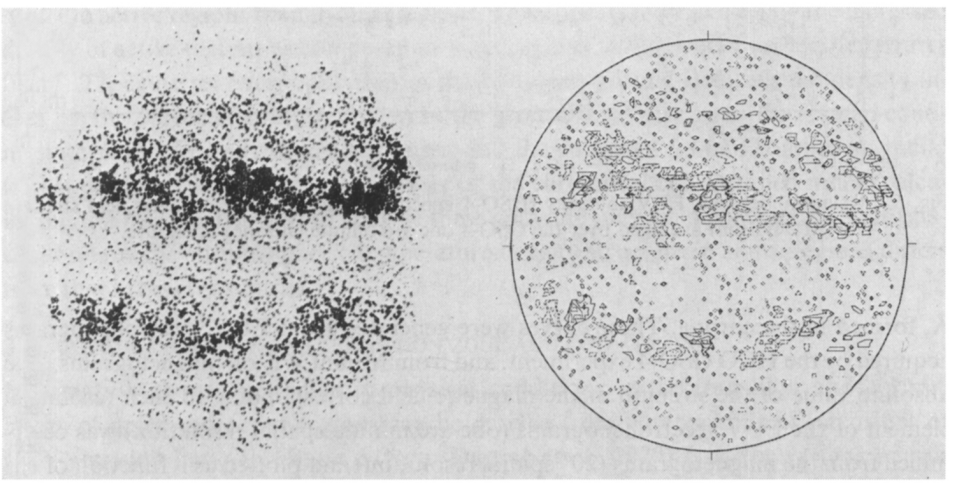

Fig. 4. OSO-4 spectroheliogram in hydrogen Lyman continuum 800 Å (left image) and a contour map of the longitudinal photospheric magnetic field strength from Mount Wilson. In the spectroheliogram the darkest areas are the regions of greatest intensity.

It is generally agreed that the increased heating is associated with strengthening of the magnetic field. EUV observations support this by revealing a rather tight relation between photospheric magnetic field strength and EUV emission in the chromosphere and corona. Figure 4 compares an EUV spectroheliogram made in the hydrogen Lyman continuum 800 Å and a Mount Wilson magnetogram. In the spectroheliogram

acquired by the HCO experiment on OSO 4, dark areas correspond to regions of enhanced brightness. As is the case with the Ca II H and K lines in the visible, there is a one-to-one correlation between EUV chromospheric emission and the strength of the photospheric magnetic field. This correlation is shown in a more quantitative manner in Figure 5, which relates the strength of the longitudinal photospheric magnetic field to the intensities of (1) the Lyman continuum 800 Å, formed in the chromosphere, (2) O VI 1032 Å, formed in the chromospheric-coronal transition area, and (3) Mg X 625

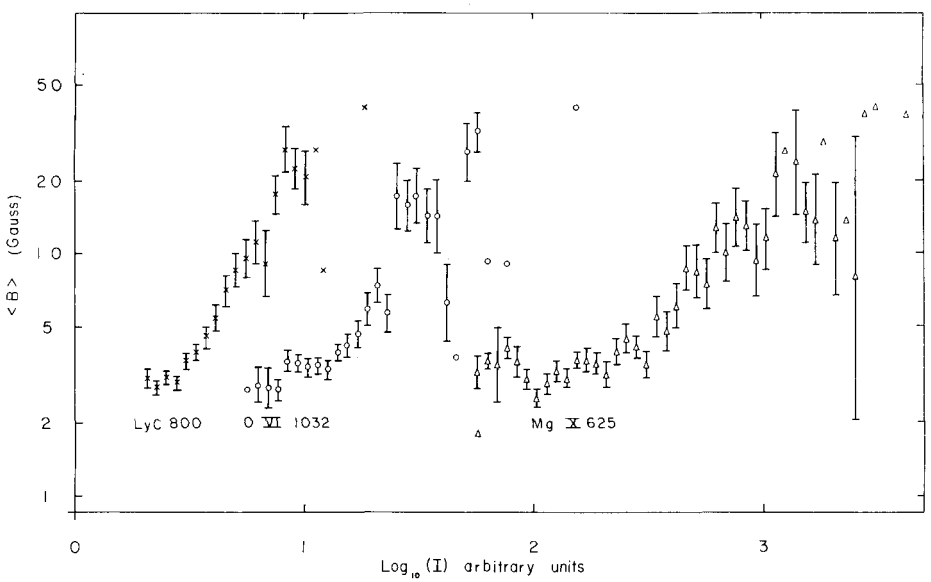

Fig. 5. Relation between EUV intensity (OSO-4 spectroheliograms) and magnetic field strength (Mt. Wilson) averaged over the OSO-4 one arc minute entrance aperature.

Å, formed in the corona. These curves were generated from EUV spectroheliograms acquired by the HCO OSO-4 experiment, and from Mount Wilson magnetograms. The absolute value of the strength of the magnetic field corresponding to each resolution element of the EUV spectroheliograms (one arc minute spatial resolution) was determined from the magnetograms (20″ spatial resolution) and plotted as a function of the EUV intensity.

The data presented in Figure 5 indicate that on the average regions of enhanced EUV emission correspond to regions of enhanced magnetic field. Since it is probable that there is a causal relationship between the strength of the photospheric magnetic field and the conditions on the overlying chromosphere and corona, it is important to perform a more sophisticated analysis of the relationship between features observed in magnetograms and EUV spectroheliograms, particularly with observations of high spatial resolution (a few arc seconds).

How do the physical conditions in active regions differ from those in quiet areas?

https://doi.org/10.1017/S0252921100089788 Published online by Cambridge University Press

Although the data that have been used for qualitative analysis were obtained by instruments with moderate spatial resolution, one-half to one arc minute, it has been possible to derive information at least on the gross differences in the physical conditions in quiet and active areas.

3. 1. Active regions in the chromosphere

Observations of chromospheric EUV lines and continua contain a wealth of information about physical conditions in the chromospheric layers of active regions. Hearn *et al.* (1969) used OSO-4 observations of the first two members of the He I resonance series, 584 Å and 537 Å, to derive chromospheric densities in quiet and active areas. On the basis of Hearn's (1969) theoretical calculations of the statistical equilibrium of a 41-level model helium atom and observed behavior of intensities of 584 Å and 537 Å, Hearn *et al.* concluded that the electron density at the temperature where the helium lines are formed, 3×10^4 K, is about 2.5 times larger in active regions than in quiet regions. For active regions the density is $\sim 10^{11}$ cm^{-3}, which corresponds to a pressure $n_e T$ of 3×10^{15}, in good agreement with active region pressures from other analyses, described below.

EUV observations of active regions made by OSO-4 and OSO-6 experiments in the hydrogen Lyman lines and continuum show some interesting trends. The color temperature derived from the slope of the Lyman continuum is approxiamtely 500 K *cooler* in active regions than in quiet regions. This appears to be caused by the increased density in active regions as compared to quiet regions. As indicated earlier, departures from LTE cause an overpopulation of the hydrogen ground level. As the density increases, the degree of overpopulation in the ground level decreases, the Lyman continuum opacity per unit volume decreases, and the emergent Lyman continuum radiation is produced in a lower, cooler layer of the chromosphere. Detailed model calculations are being performed to analyze these data and may yield considerable information on how the chromospheric temperature-density structure in active regions differs from that in quiet regions.

3. 2. Active regions in the transition zone and low corona

Information about differences in physical conditions in the transition and coronal layers of quiet and active regions can be derived from comparisons of intensities of EUV emission lines. In Figure 6 (from Dupree *et al.*, 1970) I_A/I_Q for various lines is plotted vs the temperature of line formation. The quantities I_A and I_Q are the intensities in an active and a quiet region obtained from OSO-6 spectra. The overall shape of the graph shows a continual increase of enhancement with increasing temperature. What does such a graph tell us about the physical structure of active regions? Let us look first at the points for Mg X and Si XII, for which the ratio I_A/I_Q is about 40. We pick these lines because the two million K temperature of the quiet corona is close to the temperature of their maximum abundance, so that slight changes of coronal temperature will not greatly affect their abundance. Their emission is therefore sensitive mainly to changes in electron density. Because the emission varies as the square of the den-

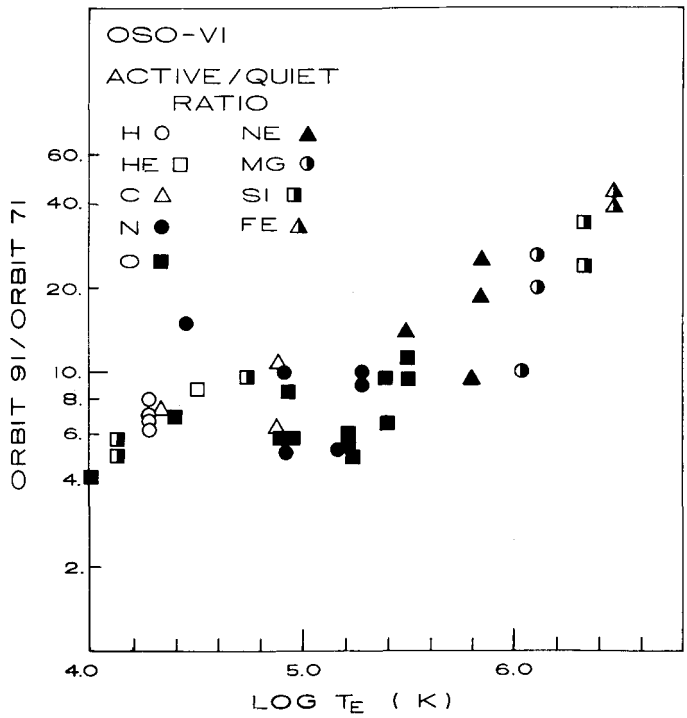

Fig. 6. Ratio of EUV intensities in an active region and a quiet region obtained by OSO 6, plotted vs temperature of maximum abundance of the ion producing the line.

sity, the enhancement by a factor of 40 implies a density increase of about 6.5 in the active region.

Lines such as Fe XVI, which are emitted most efficiently at temperatures hotter than the quiet corona, have a larger enhancement. This can be explained by an increase in the coronal temperature in active regions to about 2.5×10^6 K.

The lines formed in the upper transition zone between 10^5 and 10^6 deg are seen in the figure to fall into two more-or-less parallel bands. Fixing our attention on the upper band for the moment, we see that typical enhancements are only about a factor of 10. Hydrostatic equilibrium requires that the pressure increase be about the same as that in the low corona, so that we would have expected an enhancement by a factor of 40 like the coronal lines, other things being equal. The data are explained, however, if the total thickness of the transition zone is decreased by a factor of 4, in other words if the temperature gradient in the transition zone is increased by a factor of 4. In turn the increased temperature gradient would cause an increased conductive flux back to the chromosphere, and finally this flux must be supported by an increased mechanical heating of the corona in the active region. Thus a crude picture of the structure of active regions shows a several-fold increase of density, mechanical heating, and downward conductive flux over that in the quiet Sun, along with an increased coronal temperature (Noyes *et al.*, 1970; Reimers, 1971).

It is possible to obtain independent estimates of the density ratio in active and quiet regions from intensities of lines produced by Be-like ions. The points defining the lower curve in Figure 6 correspond to resonance lines in the beryllium and boron isoelectronic sequences. As Dupree *et al.* (1970) pointed out, these ions have a low-lying metastable level that can be populated at the expense of the ground level as the density increases, causing the Be-like resonance lines to have smaller active-region enhancements than resonance lines of ions without low-lying metastable levels. As described earlier, the relative intensities of two lines whose lower levels are respectively the metastable and the ground level are density-sensitive under certain conditions. On the left side of Figure 7 (from Munro *et al.*, 1971) the ratio of one of these density-sensitive pairs of lines, C III 1176 Å and 977 Å, is plotted as a function of the intensity of 977 Å. On the right side of Figure 7 is a similar graph for O V 760 Å and 630 Å. Since

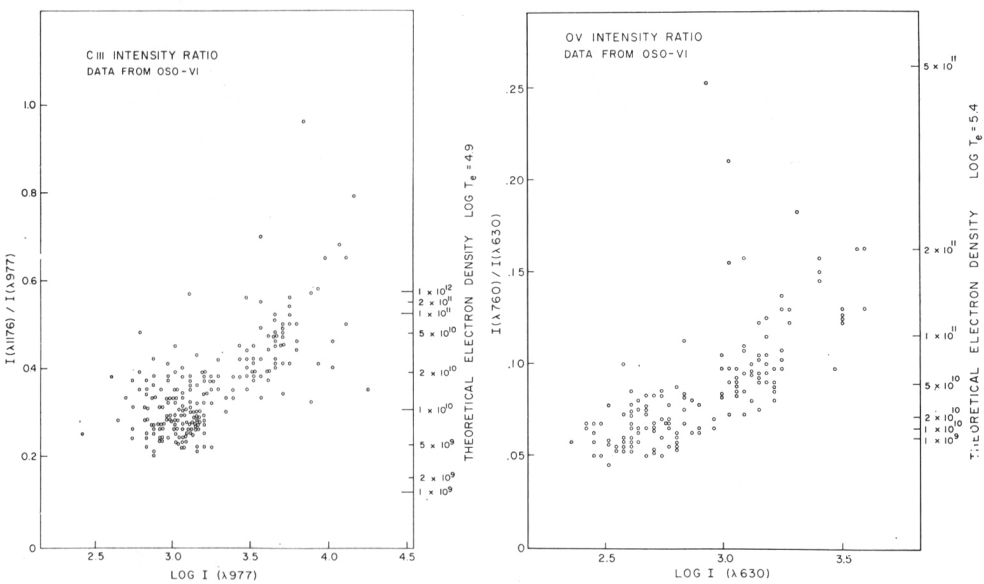

Fig. 7. (left) C III intensity ratio $I(1176\text{ Å})/I(977\text{ Å})$ as a function of intensity of resonance line 977 Å in erg cm^{-2} s^{-1} sr^{-1}. (right) O V intensity ratio $I(760\text{ Å})/I(630\text{ Å})$ as a function of intensity of resonance line 630 Å.

the intensities of 977 Å and 630 Å are larger in active regions than in quiet regions, these intensities provide a measure of activity. Although there is considerable scatter among the points in these graphs, the observed line ratios increase with increasing activity, indicating that the density in the transition zone increases with increasing activity, as expected.

The ratios of Be-like lines observed in quiet and active regions typically give active-region electron densities about 5 times larger than those in quiet regions (Dupree *et al.*, 1970; Jordan, 1971; Munro *et al.*, 1971) in good agreement with the mean density ratio inferred from enhancements of coronal EUV lines (Noyes *et al.*, 1970; Reimers, 1971;

Withbroe and Noyes, 1971). However, for individual spectra of 0.5′ areas, the transition zone electron pressures inferred by the two methods sometimes differ by a factor of 2 or more (Munro, 1971). Such disagreements probably are caused by small-scale structures in both quiet and active areas.

Using the concepts outlined above, one can construct maps of the spatial variation of pressure in the corona and the temperature gradient in the transition zone. Figure 8 shows examples of these maps. For each picture the darkest areas correspond to the regions of greatest enhancement of the parameter mapped in the picture.

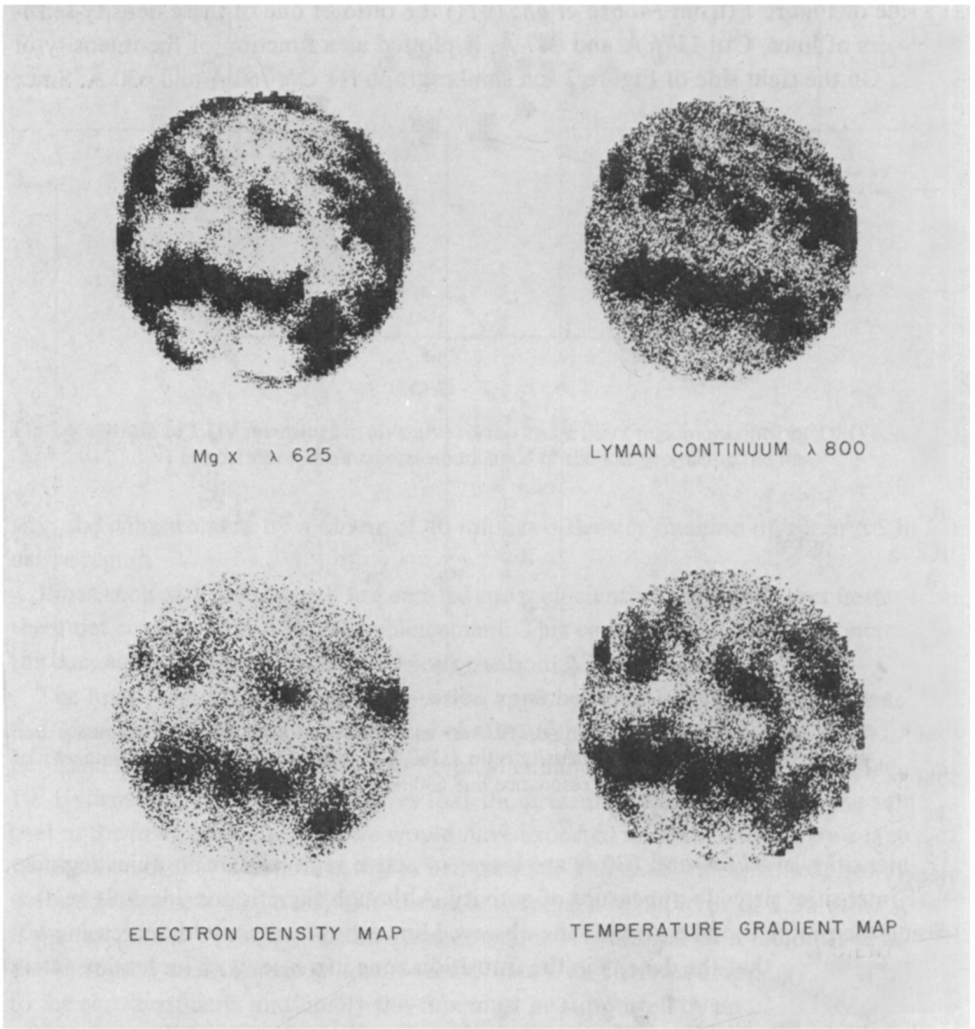

Fig. 8. (upper left) OSO-4 spectroheliogram in Mg X 625 Å. (upper right) spectroheliogram in hydrogen Lyman continuum 800 Å. (lower left) map of coronal electron density. (lower right) map of transition zone temperature gradient. In each picture the darkest areas correspond to regions of greatest enhancement.

The upper two pictures are OSO-4 spectroheliograms made in Mgx 625 Å and Lyman continuum 800 Å. The picture on the lower left is a map of the coronal electron pressure obtained by the simple expedient of removing the limb brightening from the Mgx intensities and taking the square root of the corrected intensities which, as a first approximation, are proportional to the square of the coronal electron pressure. The picture on the lower right maps the ratio of Mgx 625 Å, a coronal line, and OVI 1032 Å, a transition zone line. From the discussion given earlier this ratio is crudely proportional to the temperature gradient in the transition zone.

These pictures suggest that, as a first approximation, regions of increased chromospheric and coronal emission, increased pressure, and increased tenperature gradient in the transition zone tend to be correlated. However, there are areas where the correlation is not particularly good. This may reflect the inadequacy of the simple concepts applied to data of moderate spatial resolution.

Figure 9 (Withbroe and Noyes, 1971) shows the quantitative relationship between the coronal pressure, transition-layer temperature gradient, intensity of the Lyman continuum, and strength of the longitudinal photospheric magnetic field, all plotted as a function of the intensity of Mgx 625 Å. These curves represent mean values obtained

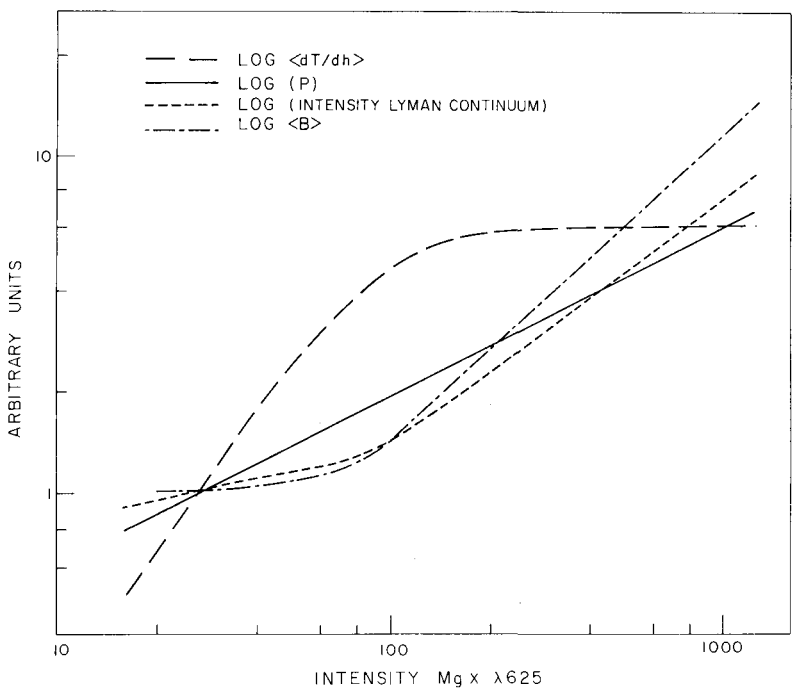

Fig. 9. Variation with Mgx intensity of transition zone temperature gradient (long dash line), transition zone pressure (solid line), Lyman continuum intensity (short dash line) and photospheric longitudinal magnetic field strength (dash-dot-line). The quietest regions are on the left and the most active on the right.

from OSO-6 spectra. Low Mgx intensities correspond to quiet areas and high Mgx intensities to active regions.

The intensity of the EUV chromosphere, the pressure at the top of the chromosphere and the strength of the photospheric magnetic field appear to be all roughly proportional. The temperature gradient in the transition zone, however, varies in a different way. The gradient increases more rapidly than the other quantities for a time, then seems to saturate at a maximum value. Perhaps turbulent mixing of the magnetic field sets an upper limit to the temperature gradient that can be maintained by thermal conduction.

Speculations of this sort are premature, however, unless data of very high spatial resolution are used. Figure 10 shows data obtained by the Naval Research Laboratory (Tousey, 1971b) with 3–5″ resolution; we see that the fine structure of active regions changes remarkably from the chromosphere to the corona. Clearly the ratio of intensities on the corona and transition zone, each integrated over a one arc min square, can give only the crudest information on actual temperature gradients.

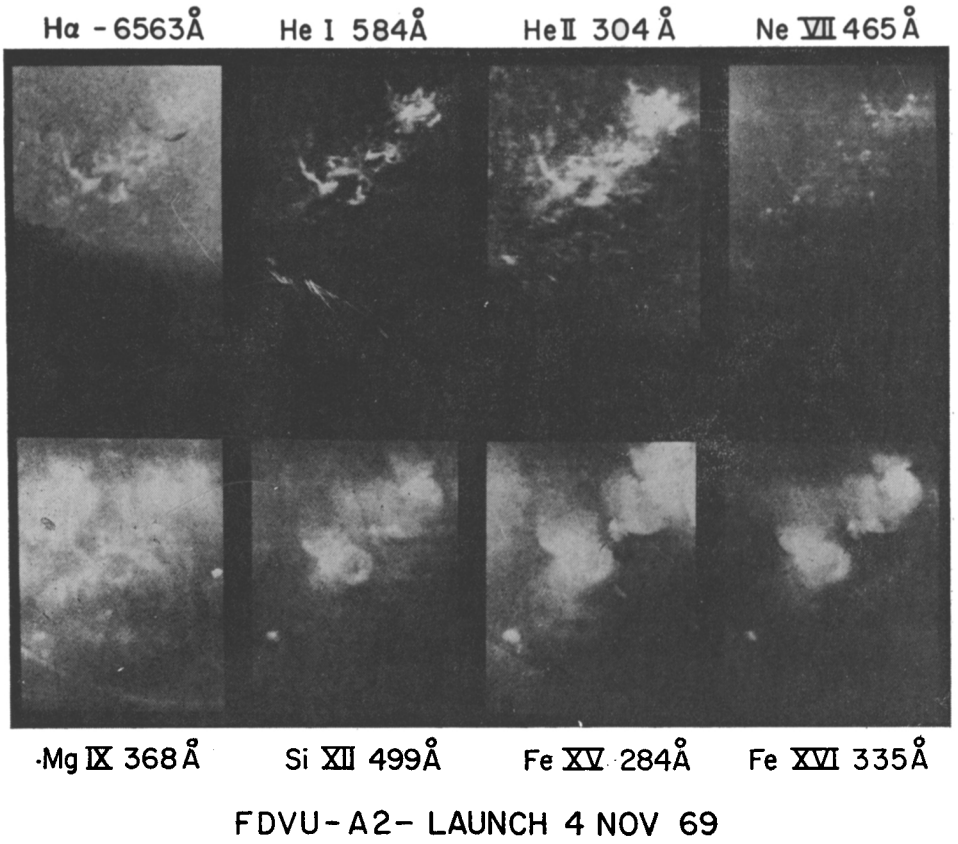

Fig. 10. Naval Research Laboratory spectroheliograms of an active region showing the variation in structure between chromospheric (Hα, HeI, HeII), transition zone (NeVII, MgIX) and coronal (SiXII, FeXV, FeXVI) lines. (Courtesy Naval Research Laboratory.)

https://doi.org/10.1017/S0252921100089788 Published online by Cambridge University Press

3. 3. 'HOLES' IN THE CORONA

Active regions represent one extreme variation of atmospheric structure from that of the quiet Sun. The other extreme is also prominent in EUV and X-ray observations. Often large extended areas are found, usually overlying regions of very weak magnetic field, in which emission in EUV coronal lines is much lower, typically by an order of magnitude, than in the average quiet area. These so-called coronal 'holes', which are in a sense the antithesis of active regions, were first observed in EUV spectroheliograms and X-ray filtergrams obtained with rocket experiments (e.g. Burton, 1968; Tousey *et al.*, 1968; Underwood and Muney, 1969). They have also been observed in EUV coronal lines with experiments on OSO 4 and OSO 6 (e.g. Reeves and Parkinson, 1970; Withbroe *et al.*, 1971). Holes are most often observed at the poles; however, they can appear anywhere on the disk. An example of a large hole extending from the equator to the pole is shown in Figure 11. The hole is clearly visible in Mg x 625 Å and Si XII 499 Å, yet is not very apparent in Lyman continuum 897 Å.

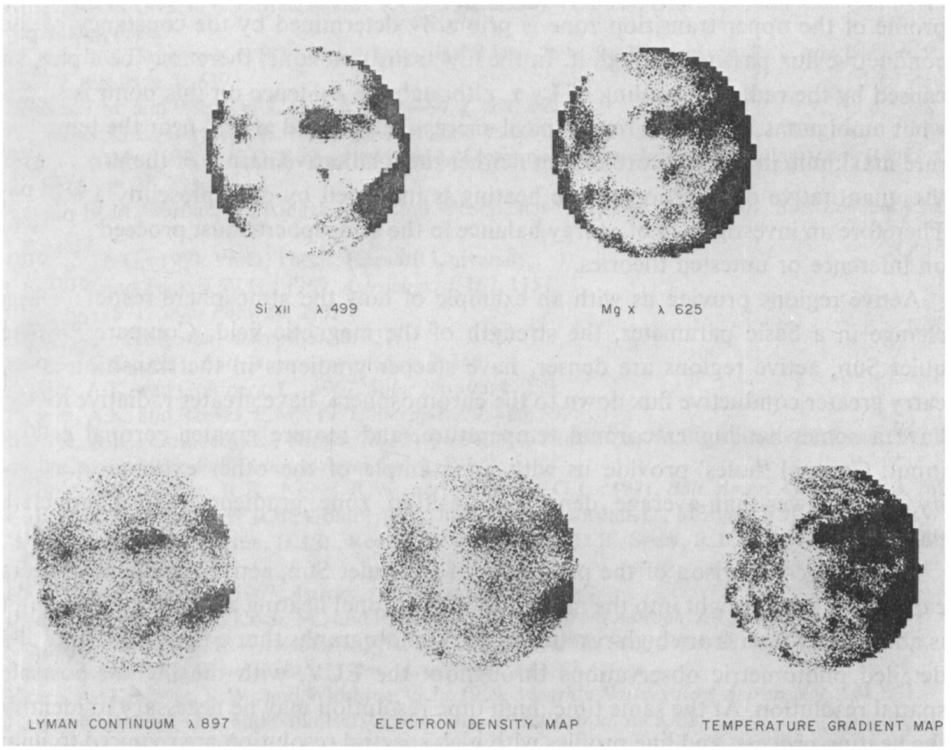

Fig. 11. OSO-4 spectroheliograms showing a coronal hole in Si XII 499 Å, Mg x 625 Å, and hydrogen Lyman continuum 897 Å. Also shown are maps of the coronal electron density and transition zone temperature gradient. In each picture the darkest areas correspond to regions of greatest enhancement. The jagged appearance of the limb results from the fact that only those data points located on the solar disk were used in constructing the pictures.

https://doi.org/10.1017/S0252921100089788 Published online by Cambridge University Press

In some areas of the hole the Mg X intensity is a factor of ten or more lower than in normal quiet areas. Although it is not apparent in the high contrast print given in Figure 11, the Si XII emission is significantly lower in the hole than elsewhere on the disk and in some areas of the hole appears to be absent. These observations suggest that the coronal temperature and density are lower in holes than in normal quiet regions. Typically the density decrease appears to be a factor of 3 (Munro and Withbroe, 1972; Wang and Withbroe, 1972; Withbroe *et al.*, 1971). The temperature gradient in the transition zone also appears to be lower in holes, by a factor of 3 to 10. This is shown qualitatively in Figure 11 by the map of the transition region temperature gradient. This map and the density map were constructed in the same manner as the maps in Figure 8.

4. Summary

In the previous pages we have reviewed many different ways of analyzing the structure of the solar atmosphere from its EUV emission. If we ignore the obvious problems of fine structure, we find that these various analyses lead to an overall structure apparently controlled by the dominant mechanisms of energy flow. Thus the temperature profile of the upper transition zone is primarily determined by the constancy of the conductive flux passing through it. In the low transition zone, there may be a plateau caused by the radiative cooling of Ly α, although the evidence on this point is somewhat ambiguous. Of course, mechanical energy is deposited at and near the temperature maximum in the low corona, but neither the qualitative nature of the process nor the quantitative distribution of the heating is indicated by data presently available. Therefore an investigation of energy balance in the atmosphere must proceed partially on inference or untested theories.

Active regions provide us with an example of how the atmosphere responds to a change in a basic parameter, the strength of the magnetic field. Compared to the quiet Sun, active regions are denser, have steeper gradients in the transition zone, carry greater conductive flux down to the chromosphere, have greater radiative losses, have a somewhat higher coronal temperature, and require greater coronal energy input. Coronal 'holes' provide us with an example of the other extreme of activity, with lower-than-average density, transition zone gradients, and conductive flux.

Although comparison of the properties of the quiet Sun, active regions, and holes can give us great insight into the mechanisms of coronal heating and energy balance, it is abundantly clear from high-resolution EUV photographs that a full solution awaits detailed photometric observations throughout the EUV, with the highest possible spatial resolution. At the same time, high time resolution may be necessary to identify the heating process, and line profiles with high spectral resolution are required to map velocity fields as well as to determine chromospheric structure. Although these observational problems are formidable indeed, the rather encouraging progress reviewed above prompts us to look ahead with some confidence. New experiments currently planned for the Apollo Telescope Mount (ATM) and for the next generation of high-

resolution Orbiting Solar Observatories, as well as improved observations from stabilized rockets, will certainly lead to a great advance in our knowledge of the physics of the solar atmosphere.

Acknowledgements

We wish to thank our colleagues in the Harvard College Solar Satellite Project, A. K. Dupree, L. Goldberg, M. Huber, W. H. Parkinson, and E. M. Reeves for numerous stimulating discussions on the solar EUV spectrum. We also wish to express our appreciation to E. Chipman, R. Munro, and J. Vernazza for their helpful suggestions and assistance. This work was supported in part by the National Aeronautics and Space Administration through contracts Nas 5-9274, and NGR 22-007-211.

References

Altschuler, M.D. and Newkirk, G., Jr.: 1969, *Solar Phys.* **9**, 131.
Athay, R.G.: 1965, *Astrophys. J.* **142**, 755.
Athay, R.G.: 1966, *Astrophys. J.* **145**, 784.
Athay, R.G.: 1970, *Astrophys. J.* **161**, 713.
Athay, R.G.: 1971, in C.J. Macris (ed.), *Physics of the Solar Corona*, D. Reidel Publ. Co., Dordrecht, Holland, p. 36.
Boland, B.C., Engstrom, S.F.T., Jones, B.B., McWhirter, R.W.P., Thonemann, P.C., and Wilson, R.: 1972, this issue, p. 639.
Bridges, J.M. and Wiese, W.L.: 1970, *Astrophys. J.* **161**, L71.
Brueckner, G.E., Bartoe, J.F., Nicholas, K.R., and Tousey, R.: 1970, *Nature* **226**, 1132.
Burton, W.M.: 1968, in K.O. Kiepenheuer (ed.), 'Structure and Development of Solar Active Regions', *IAU Symp.* **35**, 393.
Burton, W.M., Jordan, C., Ridgeley, A., and Wilson, R.: 1971, *Phil. Trans. Roy. Soc. London* **A270**, 81.
Chipman, E.G.: 1971, Ph.D. Thesis, Harvard University.
Cox, D.P. and Tucker, W.H.: 1969, *Astrophys. J.* **157**, 1157.
Cuny, Y.: 1971, *Solar Phys.* **16**, 293.
Delache, P.: 1967, *Ann. Astrophys.* **30**, 827.
Dupree, A.K.: 1971, *Bull. Amer. Astron. Soc.* **3**, 246.
Dupree, A.K. and Goldberg, L.: 1967, *Solar Physics.* **1**, 229.
Dupree, A.K. and Reeves, E.M.: 1971, *Astrophys. J.* **165**, 599.
Dupree, A.K., Goldberg, L., Huber, M., Noyes, R.W., Parkinson, W.H., Reeves, E.M., and Withbroe, G.L.: 1970, *Bull. Amer. Astron. Soc.* **2**, 191.
Dupree, A.K., Munro, R.H., Noyes, R.W., and Withbroe, G.L.: 1971, *Bull. Amer. Astron. Soc.* **3**, 260.
Gabriel, A.H., Garton, W.R.S., Goldberg, L., Jones, T.J.L., Jordan, C., Morgan, F.J., Nicholls, R.W., Parkinson, W.H., Paxton, H.J.B., Reeves, E.M., Shenton, D.B., Speer, R.J., and Wilson, R.: 1971, *Astrophys. J.* **169**, 595.
Garz, T. and Koch, M.: 1969, *Astron. Astrophys.* **2**, 274.
Garz, T., Holweger, H., Koch, M., and Richter, J.: 1969, *Astron. Astrophys.* **2**, 446.
Gingerich, O., Noyes, R.W., Kalkofen, W., and Cuny, Y.: 1971, *Solar Phys.* **18**, 347.
Hearn, A.G.: 1969, *Monthly Notices Roy. Astron. Soc.* **142**, 53.
Hearn, A.G., Noyes, R.W., and Withbroe, G.J.: 1969. *Monthly Notices Roy. Astron. Soc.* **144**, 351.
Ivanov-Khilodnyi, G.S. and Nilkolski, G.M.: 1961, *Soviet Astron. AJ* **5**, 31.
Jordan, C.: 1965, Ph.D. Thesis, London University.
Jordan, C.: 1966, *Monthly Notices Roy. Astron. Soc.* **132**, 463.
Jordan, C.: 1971, in C. de Jager (ed.), *Highlights of Astronomy*, D. Reidel Publ. Co., Dordrecht, Holland, p. 519.
Jordan, C. and Pottasch, S.R.: 1968, *Solar Phys.* **4**, 104.
Kopp, R.A. and Kuperus, M.: 1968, *Solar Phys.* **4**, 212.

Kunze, H.J.: 1972, this issue, p. 565.
Munro, R.H.: 1971, personal communication.
Munro, R. H. and Withbroe, G. K.: 1972, *Astrophys. J.*, in press.
Munro, R.H., Dupree, A.K., and Withbroe, G.L.: 1972, *Solar Phys.* **19**, 347.
Neupert, W.M.: 1967, *Solar Phys.* **2**, 294.
Nikolskii, G.M.: 1969, *Solar Phys.* **6**, 399.
Noyes, R.W.: 1971, *Ann. Rev. Astron. Astrophys.* **9**, 209.
Noyes, R.W. and Kalkofen, W.: 1970, *Solar Phys.* **15**, 120.
Noyes, R.W., Withbroe, G.L., and Kirshner, R.P.: 1970, *Solar Phys.* **11**, 388.
Parkinson, W.H. and Reeves, E.M.: 1969, *Solar Phys.* **10**, 342.
Pottasch, S.R.: 1963, *Astrophys. J.* **137**, 945.
Pottasch, S.R.: 1964, *Space Sci. Rev.* **3**, 816.
Pottasch, S.R.: 1967, *Bull. Astron. Inst. Neth.* **19**, 113.
Reeves, E.M. and Parkinson, W.H.: 1970, *Astrophys. J. Suppl.* **21**, 1.
Reeves, E. M. and Parkinson, W. H.: 1972, *Solar Phys.* **24**, 113.
Reimers, D.: 1971, *Astron. Astrophys.* **14**, 1980.
Schmidt, H.U.: 1964, in W.N. Hess (ed.), *The Physics of Solar Flares*, NASA SP-50, p. 107.
Simon, G.W. and Noyes, R.W.: 1972, *Solar Phys.* **22**, 450.
Speer, R.J., Garton, W.R.S., Goldberg, L., Jones, T.J.L., Morgan, J.F., Nicholls, R.W., Parkinson, W.H., Paxton, H.J.B., Reeves, E.M., Shenton, D.B., and Wilson, R.: 1970, *Nature* **226**, 249.
Thomas, R.N. and Athay, R.G.: 1961, *Physics of the Solar Chromosphere*, Interscience, New York.
Tousey, R.: 1971a, *Phil. Trans. Roy. Soc.* **270**, 59.
Tousey, R.: 1971b, in F. Labuhn and R. Lüst (eds.), 'New Techniques in Space Astronomy', *IAU Symp.* **41**, 233.
Tousey, R., Purcell, J.D., Auston, W.E., Garrett, D.L., and Widing, K.G.: 1964, in J.P. Muller (ed.), *Space Res.*, North-Holland Publ. Co., Amsterdam, 703.
Tousey, R., Sandlin, G.D. and Purcell, J.D.: 1968, in K.O. Kiepenheuer (ed.), 'Structure and Development of Solar Active Regions', *IAU Symp.* **35**, 411.
Ulmschneider, P.H.: 1970, *Astron. Astrophys.* **4**, 144.
Underwood, J.H. and Muney, W.S.: 1967, *Solar Phys.* **1**, 129.
Vernazza, J. and Avrett, E.H.: 1972, in preparation.
Vernazza, J. and Noyes, R.W.: 1972, *Solar Phys.* **22**, 358.
Wang, Y. M. and Withbroe, G. L.: 1972, submitted to *Solar Phys.*
Widing, K.G., Purcell, J.O., and Sandlin, G.D.: 1970, *Solar Phys.* **12**, 52.
Withbroe, G.L.: 1970a, *Solar Phys.* **11**, 42.
Withbroe, G.L.: 1970b, *Solar Phys.* **11**, 208.
Withbroe, G.L.: 1971a, *Solar Phys.* **18**, 458.
Withbroe, G. L.: 1971b, *Proc. Mensel Symp. on Astrophys.*, NBS special Report **353**, 127.
Withbroe, G.L. and Noyes, R.W.: 1971, *Bull. Amer. Astron. Soc.* **3**, 265.
Withbroe, G. L., Dupree, A. K., Goldberg, L., Huber, M., Noyes, R. W., Parkinson, W. H., and Reeves, E. M.: 1972, *Solar Phys.* **21**, 272.

DISCUSSION

M. Kuperus: When you mention an average temperature increase of 0.5×10^6 K do you mean that there is a well defined increase above active regions with a small spread around this value or do you find the kind of values from 0 to lets say 1 or 1.5×10 K ?

R.W. Noyes: We suspect that the amount of temperature increase is greater, the brighter (i.e. the denser) the active region. However, the data in this point are weak because only a few emission lines accessible to the Harvard OSO experiments (e.g. Fe XV 417, Fe XVI 361, and Fe XVI 335) are strongly sensitive to temperature, and these lines are complicated by blends.

C. Jordan: In your talk you have said that using the limb-to-disk method we cannot distinguish between models with similar steep gradients. Using optically thin lines alone this is true; our scatter is $\pm 1.5''$. However we can use our disk intensities to produce a model from which we can calculate optical depths. Using lines which are optically thin at the centre of the disk but which became optically thick at the limb we can distinguish between models which have gradient differences of only a factor of two (See Burton *et al.*, 1971), through the difference in electron pressures assumed.

R.A. Kopp: Do the extensive regions on the disk with negligible emission in Mg x 625 appear dark in other coronal EUV lines as well? If so, can upper limits be placed on the temperature and electron density in these coronal regions?

G.L. Withbroe: The low emission areas of 'holes' observed in Mg x are also areas of low emission in Si XII and Fe XVI. In Mg x the intensity is lower by an order of magnitude over normal quiet areas. The Si XII and Fe XVI emission in holes is undectectable because of low signal levels. We have not yet placed limits on the decrease in the coronal temperature, but the density decrease inferred from Mg x is about a factor of 3. [We have now determined that the coronal temperature is about 10^6 K in holes.]

A.H. Gabriel: Can one correlate your holes in the corona with the phenomena observed beyond the limb during eclipses in white light and Lyman-α? These gaps are seen up to over 1/3 $R_\odot$ in height and indicate a density drop of a factor ~ 3 with perhaps a lowering of the temperature also.

G.L. Withbroe: The large 'hole' or gap observed at the limb on March 7, 1970 in white light and Lyman-α eclipse photographs is also visible in Mg x 625 at the limb on March 7 and on the disk before the eclipse (Withbroe *et al.*, *Solar Phys.*, **21** (1971), 272). The Mg x data indicate that the density decrease was about a factor of 3 for this feature.

B. Woodgate: Do the holes in the corona show up as density decreases as measured by the Be-like line ratios?

R. W. Noyes: Yes, observations in the Be-like C III and O V lines suggest that the density where these lines are formed is lower than in the normal quiet sun. Detailed comparison between density in holes inferred by the different methods described in the paper show discrepancies, however, suggesting that inhomogeneities on a scale below 30″ complicate the picture.

G. Noci: The electron temperature of the solar corona, deduced by the total intensities of the UV lines that you showed in the first slide (~ 1.5–2×10^6 K) gives a higher brightness temperature than observed at metric wavelengths ($\sim 1 \times 10^6$ K). Since the solar corona is optically thick in this spectral region, this can only be explained, in my opinion, by assuming an absence of spherical symmetry and a different contribution to UV emission than to radio emission by regions at different temperatures.

L. P. Van Speybroeck: The X-ray photographs obtained by the A. S. and E. group result in higher temperatures at lower altitudes than given in the analysis presented here. This also results in a much higher heat conduction ($\sim T^{7/2}$/scale height) if interpreted by a simple radial model. This is another indication of the lack of homogeneity, which of course was stressed by Dr Noyes. This probably indicates temperature structure across the magnetic field which inhibits the heat conduction, to be consistent with the values observed in the UV. This model is also consistent with the lower microwave emission remarked upon earlier.